Iranian Journal of Science and Technology, Transactions of Mechanical Engineering
https://doi.org/10.1007/s40997-023-00705-2

RESEARCH PAPER

Nonlinear Dynamic Response of Functionally Graded Porous Beams Under a Moving Mass Using Reddy's Beam Theory

Van-Long Nguyen[1] · Minh-Tu Tran[1] · Thanh-Binh Chu[1] · Tuan-Anh Nguyen[2] · Van-Loi Nguyen[1]

Received: 11 June 2023 / Accepted: 17 August 2023

Abstract

This work presents solutions for the nonlinear dynamic features of beams with a Winkler-Pasternak foundation under a traveling mass, employing Reddy's beam theory. The beam is made from a functionally graded porous material (FGPM) with three patterns of porosity distribution considered, including symmetric, asymmetric, and uniform distributions. The system of governing equations of the beam is developed based on the Ritz procedure and Lagrange's equation. The nonlinear responses of the FGPM beam are then obtained via the Runge–Kutta scheme. Verifications are presented to confirm the accuracy and reliability of the present model with the literature. The effects of material parameters, geometry parameters, elastic foundation, boundary conditions, and moving mass parameters on the dynamic features of the FGPM beam are studied via parametric studies. The linear and nonlinear responses of the beam also are compared. Based on numerical results, it can be disclosed that the porosity distribution patterns and coefficient play an important role in the nonlinear dynamic response. The non-uniform symmetric porosity distribution pattern offers the best performance, i.e. the highest fundamental frequency and the lowest dynamic deflection.

Keywords Dynamic responses · FGPM beam · Moving mass · Reddy's beam theory

1 Introduction

The study of dynamic features of structures has been a critical field and main interest for past years. Many studies on the dynamic behaviors of engineering structures can be found in the existing literature (Reddy 2003; Tran et al. 2017; Moghaddasi and Kiani 2022; Phu et al. 2022; Bagheri et al. 2023). Recently, advanced materials such as functionally graded material (FGM) and functionally graded porous material (FGPM) have been applied in many engineering fields (aerospace, automobile, nuclear engineering, mechanical engineering, civil engineering, and defense area) (Chen et al. 2016; Nguyen and Hoang 2019; Boggarapu et al. 2021; Tung et al. 2021; Vinh et al. 2022). In particular, lightweight structures made of FGPM (metal foam) can offer unique characteristics for various applications in aerospace, automobile, and civil engineering (Badiche et al. 2000; Banhart 2001; Smith et al. 2012). With outstanding energy-absorbing capability, the FGPM is a potential candidate for engineering structures under dynamic loadings. Moreover, the material properties of the FGPM can vary in one or more directions; as a result, they can be appropriately adjusted for different purposes and improvement of the structure performance (Chen et al. 2016; Dang et al. 2022).

The problem of moving loads is a crucial topic of structural dynamics. This issue frequently arises in various engineering applications, such as roadways, railroads, runways, guideways, bridges, tunnels, pipelines, and overhead cranes, … all of which are related to moving load and moving mass problems. Numerous works focused on the mechanical behaviors of beam problems subjected to the moving load, where inertial effects are neglected, have been published (Şimşek 2010a; Michaltsos 2002; Samani and Pellicano 2009; Jorge et al. 2015; Froio et al. 2018; Sheng and Wang 2017). For the moving mass problem, in contrast, the inertial effect of the moving mass could not be ignored, and this topic is attracted many authors in the last few decades. For example, using an analytical–numerical approach,

✉ Van-Loi Nguyen
loinv@huce.edu.vn

[1] Department of Strength of Materials, Hanoi University of Civil Engineering (HUCE), 55 Giai Phong road, Hanoi, Vietnam

[2] Department of Civil Engineering, Vinh University, 182 Le Duan, Vinh City, Vietnam

Published online: 15 September 2023

Akin and Mofid (1989) determined the dynamic features of beams under a transverse moving mass, where various boundary conditions were included. Foda and Abduljabbar (1998) utilized the Green function method and the classical beam theory to study the dynamic features of the beam under a moving mass. On the basis of different beam models, reproducing the kernel particle method, Kiani et al. (2009) investigated the influence of several factors on the dynamic response of beams under a moving mass. Using large deflection theory, including von Kárman nonlinearity, Mamandi and Kargarnovin (2011) analyzed the dynamic features of an inclined beam subjected to a moving mass/force, where the Timoshenko beam theory was utilized. Jiang (2011) studied the dynamic features of an undamped beam carrying an accelerating mass by using the reverberation-ray matrix method. Esen (2011, 2017) analyzed the dynamic responses of beams subjected to a moving mass, where the classical beam theory model and finite element (FE) method were used. Also by using FEM, this author then investigated the dynamic behaviors of microbeams under a moving mass within the framework of FSDT and the results have been presented in (Esen 2020a). Other remarkable works related to engineering structures under the moving mass, can be found in the literature (Fryba and Frýba 1999; Nikkhoo et al. 2007; Ouyang 2011; Esen 2013, 2015, 2020b; Esen and Koç 2015a, 2015b; Koç and Esen 2017; Koç et al. 2018; Özarpa and Esen 2020; Shokouhifard et al. 2020a; Chen et al. 2021).

The use of advanced materials (i.e., FGM and FGPM) for engineering structures under the moving load and moving mass can also be found in the existing literature; several noticeable works are listed here. For example, Şimşek and Kocatürk (2009) presented free vibration and dynamic features of the beam under a moving harmonic load, where the simply supported beam made of FGM and classical beam theory were studied. Also, Şimşek (2010b) analyzed the forced vibration of FGM beams under a traveling mass, where different beam theories were considered, including classical, Timoshenko, and Reddy's beam theory models. Esen et al. conducted axial and transverse vibration analysis of FGM beams under a decelerating/ accelerating mass using the FE method; in their study, the results of two different beam models were compared in Esen et al. (2018), and the thermal effect was considered in the work of (Esen 2019a). Interestingly, Esen (2019b) presented a modified FE method for analyzing the vibrations of an FGM beam under a traveling mass with a variable velocity; the beam resting a two-parameter foundation was considered. Using the higher-order beam theory and the Newmark method, Wang et al. (2019) studied the vibrational characteristic of a composite beam subjected to two successive traveling masses. Based on the quasi-3D theory and FEM, Vu et al. (2021) investigated the influence of material, foundation, and loading parameters on the vibrational characteristics of bidirectional FG sandwich beams carrying a moving mass. Esen et al. (2023) used FEM and Newmark method to explore the dynamic behaviors of the FG beam with the elastic foundation and under a moving mass. Using FEM, Nguyen et al. (2022a) carried out comprehensive parametric studies to examine the influence of beam geometry parameters and moving mass velocity on the dynamic behavior of three-phase bidirectional FG sandwich beams. Applying the Lagrange equation and Ritz procedure, Akbaş et al. (2021) analyzed the dynamic response of FG porous microbeam using the classical beam model. Alimoradzadeh and Akbas (2022) examined the effect of material, viscoelastic foundation, and moving mass on the nonlinear response of FG beams under a moving mass in thermal environments. Especially, Bahranifard et al. (2020) presented transient responses of curved beams in a thermal environment subjected to a concentrated moving load, where the beam made of functionally graded graphene platelet reinforced composite (FG-GPLRC) was considered; and the FSDT, Chebyshev–Ritz method, and Newmark's scheme were employed in the simulation. Shokouhifard et al. (2020b) studied the dynamic behavior of an inclined FGM beam with various boundary conditions subjected to a moving mass. They used the FSDT, FE method to develop and solve the governing equations of the FGM beam. Bahranifard et al. (2022a) presented the nonlinear vibrational analysis and responses of sandwich beams with a porous core and two GPLRC layers under a concentrated moving load. Also, note that studies on FGPM structures under moving load and moving mass are very limited in the literature. For example, Chen et al. (2016) presented free vibration and dynamic responses of beams under a moving load, where the beam made of FGPM with three kinds of porosity distributions was studied. Using the Newmark method and Chebyshev–Ritz technique, Wang et al. (2020) conducted a study on transient response of FG porous sandwich beams under a traveling mass, where the non-uniformly distributed traveling mass and high-order beam theory is considered. Recently, Tian et al. (2023) also conducted a nonlinear dynamic analysis of plates under a moving mass, where the plate made of FGPM was studied.

Until now, several beam theories have been introduced to simulate engineering structures (Şimşek 2010b; Wang et al. 2000; M Şïmşek, T Kocatürk 2007). The Euler–Bernoulli beam theory was the first to be proposed, but it is suitable for thin and long beams. The first-order shear deformation beam theory (i.e., FSDT—Timoshenko beam theory) was subsequently introduced to consider the effect of shear deformation. However, this FSDT theory requires the use of a shear correction factor (SCF) because it assumes the shear deformation is a uniform distribution across the thickness direction. Determining the SCF is challenging because it depends on various factors such as loading, material characteristics, geometry parameters, and boundary conditions. High-order shear deformation theories (HSDTs) were subsequently proposed (Şimşek 2010b; Wang et al. 2000; M Şi̇mşek, T Kocatürk 2007). These theories yield more accurate results by assuming higher-order variations of in-plane displacement components across the beam thickness. Among the HSDTs, Reddy's third-order shear deformation beam theory (i.e., Reddy's TSDT—Reddy's beam theory) has been widely used due to its simplicity and computational efficiency (Wang et al. 2000). Therefore, Reddy's beam theory is employed in the simulation conducted in this study.

Based on the literature survey, the nonlinear dynamic features of the FGPM beam resting an elastic foundation under a moving mass, using Reddy's beam theory, have been yet explored. The motivation and novelty of the present work are: (a) nonlinear analysis of beams subjected to a moving mass using Reddy's TSDT is considered, (b) the beam made of functionally graded porous material (FGPM) with three distribution patterns (symmetric, asymmetric, uniform distributions) is studied. Note that, in the present study, the governing equations of the FGPM beam are developed on the basis of the Ritz procedure, Lagrange's equation, and Reddy's TSDT. The nonlinear dynamic features of the FGPM beam under the moving mass and load are then obtained via the Runge–Kutta scheme. Three kinds of porosity distribution are studied, including uniform (T1), symmetric (T2), and asymmetric (T3) distributions. The influences of different factors (i.e., material, geometry, elastic foundation, boundary conditions, and moving mass parameters) on the dynamic features of FGPM beams are investigated through parametric studies.

2 FGPM Beam Model Under a Moving Mass

Consider an FGPM beam of length L in x direction, width b, and height h in y and z directions, as described in Fig. 1. The beam resting on Pasternak's elastic foundation and subjected to a moving mass M, which travels with a constant velocity v_M, in the x-direction, the moving mass position is determined by $x_M(t) = v_M t$. The assumptions adopted in this study are: (i) the considered problem is geometrically nonlinear with von Kármán nonlinearity, (ii) the initial conditions of the beam are zeros, (iii) dimensions of the moving mass are omitted in comparison with those of the beam, so the problem can be considered as a point moving mass.

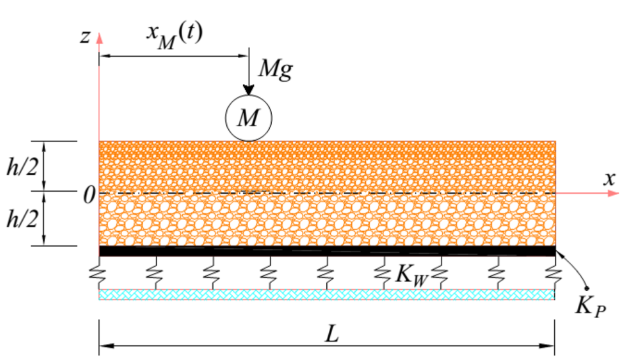

Fig. 1 An FGPM beam model with an elastic foundation under a moving mass

The beam is made from the porous material (functionally graded porous beam – FGPM beam), and three kinds of porosity distributions (T1, T2, T3) are studied, as shown in Fig. 2. (E, G, ρ) are elastic Young's modulus, shear modulus, and mass density, respectively; they can be determined as follows (Chen et al. 2016; Dang et al. 2022; Barati and Zenkour 2017; Nguyen et al. 2023):

Uniform distribution (T1 pattern):

$$\{E(z), G(z)\} = \{E_1, G_1\}(1 - e_0\chi);$$
$$\rho = \rho_1\sqrt{1 - e_0\chi} \text{ with } \chi = \frac{1}{e_0} - \frac{1}{e_0}\left(\frac{2}{\pi}\sqrt{1 - e_0} - \frac{2}{\pi} + 1\right)^2 \tag{1}$$

Symmetric distribution (T2 pattern):

$$\begin{aligned}\{E(z), G(z)\} &= \{E_1, G_1\}\left[1 - e_0\cos\left(\frac{\pi z}{h}\right)\right];\\ \rho(z) &= \rho_1\left[1 - e_m\cos\left(\frac{\pi z}{h}\right)\right]\end{aligned} \tag{2}$$

Asymmetric distribution (T3 pattern):

$$\begin{aligned}\{E(z), G(z)\} &= \{E_1, G_1\}\left[1 - e_0\cos\left(\frac{\pi z}{2h} + \frac{\pi}{4}\right)\right];\\ \rho(z) &= \rho_1\left[1 - e_m\cos\left(\frac{\pi z}{2h} + \frac{\pi}{4}\right)\right]\end{aligned} \tag{3}$$

in which the porosity coefficients (e_0 and e_m) are given by

$$\begin{aligned}&e_0 = 1 - E_2/E_1 = 1 - G_2/G_1;\\ &e_m = 1 - \sqrt{1 - e_0}\end{aligned} \tag{4}$$

where (E_1, G_1, ρ_1) and (E_2, G_2, ρ_2) are the maximum and minimum values of the corresponding material properties of the beam. Also, note that Poisson's ratio is assumed to be constant in the present study (Ashby et al. 2000).

3 Energy Expressions

Based upon Reddy's beam theory (Wang et al. 2000), the displacement components (u, w) of the beam are defined by:

$$\begin{aligned}u(x,z,t) &= u_0(x,t) + z\theta_x(x,t) - \frac{4}{3h^2}z^3\left(\theta_x + w_{0,x}\right);\\ w(x,z,t) &= w_0(x,t)\end{aligned} \tag{5}$$

where u_0, w_0 axial and transverse displacement components of a point on the beam's middle plane, respectively, θ_x is

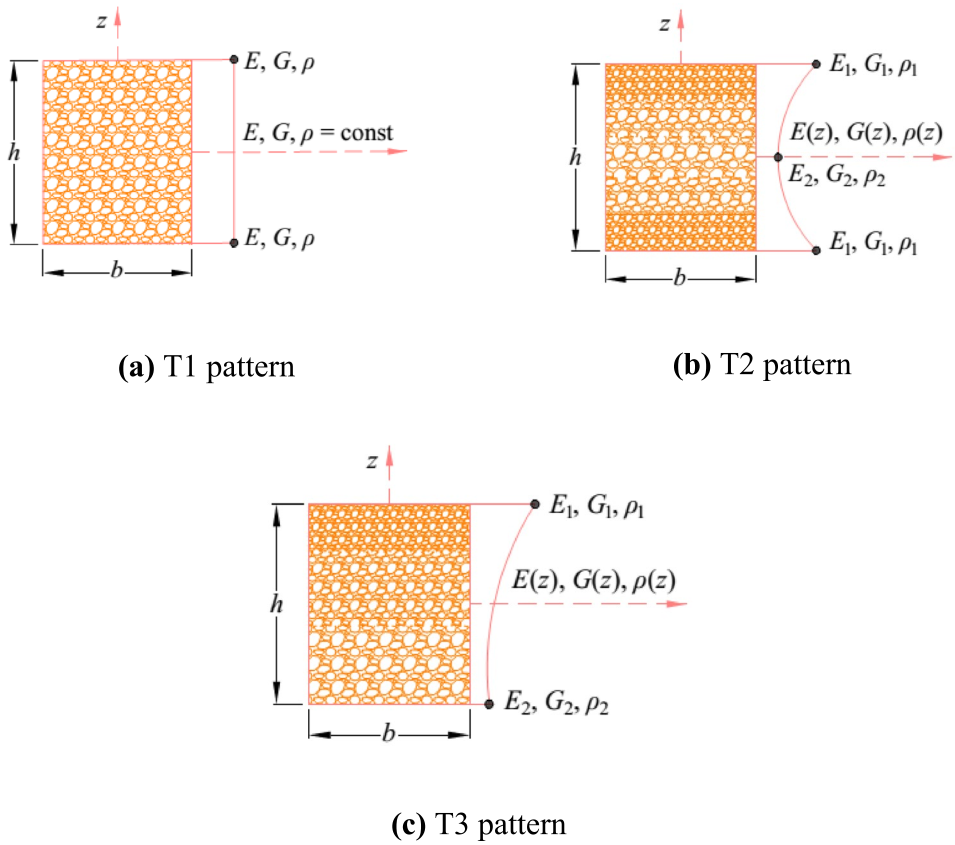

Fig. 2 Three patterns of the porosity distribution of the FGPM beam

the rotation of the beam's cross-section, t is the time variable. The subscript (,) stands for the partial derivative. The strain–displacement relations of the beam, including von Kármán geometric nonlinear terms, are computed by:

$$\begin{aligned}\varepsilon_x &= u_{0,x} + \frac{1}{2}w_{0,x}^2 + z\theta_{x,x} - \frac{4}{3h^2}z^3\left(\theta_{x,x} + w_{0,xx}\right)\\ &= u_{0,x} + \frac{1}{2}w_{0,x}^2 + \left(z - \frac{4}{3h^2}z^3\right)\theta_{x,x} - \frac{4}{3h^2}z^3 w_{0,xx};\\ \gamma_{xz} &= \left(1 - \frac{4}{h^2}z^2\right)\left(\theta_x + w_{0,x}\right)\end{aligned} \tag{6}$$

For the FGPM beam, the stress–strain relationships are the following:

$$\begin{aligned}\sigma_x &= Q_{11}\varepsilon_x = E(z)\varepsilon_x;\\ \tau_{xz} &= Q_{66}\gamma_{xz} = G(z)\gamma_{xz}\end{aligned} \tag{7}$$

The strain energy of the FGPM beam can be defined by:

$$\begin{aligned}U_B &= \frac{1}{2}\int_0^L \int_{(A)} \left(\sigma_x\varepsilon_x + \tau_{xz}\gamma_{xz}\right) dAdx\\ &= \frac{1}{2}\int_0^L \int_{(A)} \left[\begin{array}{l} E(z)\left[u_{0,x} + \frac{1}{2}w_{0,x}^2 + \left(z - \frac{4}{3h^2}z^3\right)\theta_{x,x} - \frac{4}{3h^2}z^3 w_{0,xx}\right]^2\\ +G(z)\left(1 - \frac{4}{h^2}z^2\right)^2\left(w_{0,x} + \theta_x\right)^2 \end{array}\right] dAdx\\ &= \frac{1}{2}\int_0^L \left[\begin{array}{l} A_{11}u_{0,x}^2 + \frac{A_{11}}{4}w_{0,x}^4 + A_{11}w_{0,x}^2 u_{0,x} + G_{11a}\theta_{x,x}^2 + G_{11b}w_{0,xx}^2\\ +2D_{11a}u_{0,x}\theta_{x,x} + D_{11a}w_{0,x}^2\theta_{x,x} + 2D_{11b}u_{0,x}w_{0,xx} + D_{11b}w_{0,x}^2 w_{0,xx}\\ +2G_{11c}\theta_{x,x}w_{0,xx} + F_{55}\left(w_{0,x}^2 + \theta_x^2 + 2w_{0,x}\theta_x\right) \end{array}\right] bdx\end{aligned} \tag{8}$$

where

$$
\begin{aligned}
A_{11} &= \int_{-h/2}^{h/2} E(z)dz; \\
D_{11a} &= \int_{-h/2}^{h/2} E(z)\left(z - \frac{4}{3h^2}z^3\right)dz; \\
D_{11b} &= \int_{-h/2}^{h/2} E(z)\left(-\frac{4}{3h^2}z^3\right)dz; \\
G_{11a} &= \int_{-h/2}^{h/2} E(z)\left(z - \frac{4}{3h^2}z^3\right)^2 dz; \\
G_{11b} &= \int_{-h/2}^{h/2} E(z)\left(-\frac{4}{3h^2}z^3\right)^2 dz; \\
G_{11c} &= \int_{-h/2}^{h/2} E(z)\left(z - \frac{4}{3h^2}z^3\right)\left(-\frac{4}{3h^2}z^3\right)dz; \\
F_{55} &= \int_{-h/2}^{h/2} G(z)\left(1 - \frac{4}{h^2}z^2\right)^2 dz
\end{aligned} \tag{9}
$$

The potential energy of the Winkler-Pasternak elastic foundation can be given by:

$$
U_F = \frac{1}{2}\int_0^L \left(K_W w_0^2 + K_P w_{0,x}^2\right) b dx \tag{10}
$$

in which K_W is the Winkler stiffness coefficient, K_P is the shear stiffness coefficient. The kinetic energy of the FGPM beam is determined by:

$$
\begin{aligned}
K_B &= \frac{1}{2}\int_0^L \int_{(A)} \rho(z)\left(\dot{u}^2 + \dot{w}^2\right) dA dx \\
&= \frac{1}{2}\int_0^L \begin{bmatrix} I_A\left(\dot{u}_0^2 + \dot{w}_0^2\right) + I_{Ga}\dot{\theta}_x^2 + I_{Gb}\dot{w}_{0,x}^2 \\ +2I_{Da}\dot{u}_0\dot{\theta}_x + 2I_{Db}\dot{u}_0\dot{w}_{0,x} + 2I_{Gc}\dot{\theta}_x\dot{w}_{0,x} \end{bmatrix} b dx
\end{aligned} \tag{11}
$$

where the sign (.) represents the derivative in the time variable. Moments of inertia in Eq. (11) are determined as follows:

$$
\begin{aligned}
I_A &= \int_{-h/2}^{h/2} \rho(z)dz; \\
I_{Da} &= \int_{-h/2}^{h/2} \rho(z)\left(z - \frac{4}{3h^2}z^3\right)dz; \\
I_{Db} &= \int_{-h/2}^{h/2} \rho(z)\left(-\frac{4}{3h^2}z^3\right)dz; \\
I_{Ga} &= \int_{-h/2}^{h/2} \rho(z)\left(z - \frac{4}{3h^2}z^3\right)^2 dz; \\
I_{Gb} &= \int_{-h/2}^{h/2} \rho(z)\left(-\frac{4}{3h^2}z^3\right)^2 dz; \\
I_{Gc} &= \int_{-h/2}^{h/2} \rho(z)\left(z - \frac{4}{3h^2}z^3\right)\left(-\frac{4}{3h^2}z^3\right)dz
\end{aligned} \tag{12}
$$

The kinetic energy of the moving mass is determined by (Şimşek 2010b; Wang et al. 2019):

$$
\begin{aligned}
K_M &= \frac{1}{2}c(t)M\left[\left(\dot{u}_0 + v_M\right)^2 + \left(\dot{w}_0 + v_M w_{0,x}\right)^2\right]\Big|_{x=x_M(t)} \\
&= \frac{1}{2}c(t)M\left[\dot{u}_0^2 + 2v_M\dot{u}_0 + v_M^2 + \dot{w}_0^2 + 2\dot{w}_0 v_M w_{0,x} + v_M^2 w_{0,x}^2\right]\Big|_{x=x_M(t)}
\end{aligned} \tag{13}
$$

in which $c(t)$ is a time-dependent function given by:

$$
c(t) = \begin{cases} 1, & 0 \le t \le \frac{L}{v_M} \\ 0, & t > \frac{L}{v_M} \end{cases} \tag{14}
$$

The potential of the moving mass is the following:

$$
W = Mgw_0(x_M, t)c(t) \tag{15}
$$

where $g = 9.81$ m/s^2, is the gravitational acceleration. From Eqs. (8), (10), (11), (13), (15), the energy functional of the FGPM beam can be determined by (Şimşek 2010b):

$$
\Pi = \left(K_B + K_M\right) - \left(U_B + U_F + W\right) \tag{16}
$$

4 Ritz Procedure

To develop the governing equations of the FGPM beam subjected to the moving mass, the Ritz procedure is utilized in the present study. Firstly, the displacement components (u_0;

Table 1 Admissible functions of the beam

Boundary conditions	Geometry boundary conditions	$F_j^u(x)$	$F_j^w(x)$	$F_j^\theta(x)$
CC-IM	$u_0 = w_0 = w_{0,x} = \theta_x = 0$ at $x=0$ and $x=L$	$\left(\frac{x}{L}\right)^j\left(1-\frac{x}{L}\right)$	$\left(\frac{x}{L}\right)^{j+1}\left(1-\frac{x}{L}\right)^2$	$\left(\frac{x}{L}\right)^j\left(1-\frac{x}{L}\right)$
CS-IM	$u_0 = w_0 = w_{0,x} = \theta_x = 0$ at $x=0$ and $u_0 = w_0 = 0, \theta_x \neq 0$ at $x=L$	$\left(\frac{x}{L}\right)^j\left(1-\frac{x}{L}\right)$	$\left(\frac{x}{L}\right)^{j+1}\left(1-\frac{x}{L}\right)$	$\left(\frac{x}{L}\right)^j$
SS-IM	$u_0 = w_0 = 0, \theta_x \neq 0$ at $x=0$ and $x=L$	$\left(\frac{x}{L}\right)^j\left(1-\frac{x}{L}\right)$	$\left(\frac{x}{L}\right)^j\left(1-\frac{x}{L}\right)$	$\left(\frac{x}{L}\right)^{j-1}$
CF	$u_0 = w_0 = w_{0,x} = \theta_x = 0$ at $x=0$; $u_0 \neq 0, w_0 \neq 0, \theta_x \neq 0$ at $x=L$;	$\left(\frac{x}{L}\right)^j$	$\left(\frac{x}{L}\right)^{j+1}$	$\left(\frac{x}{L}\right)^j$

w_0; θ_x) are assumed to be the polynomial series as follows (Xie et al. 2020):

$$u_0(x,t) = \sum_{j=1}^{N} Q_{1j}(t)F_j^u(x); \quad w_0(x,t) = \sum_{j=1}^{N} Q_{2j}(t)F_j^w(x); \quad \theta_x(x,t) = \sum_{j=1}^{N} Q_{3j}(t)F_j^\theta(x) \tag{17}$$

where $Q_{ij} = \{Q_{1j}(t), Q_{2j}(t), Q_{3j}(t)\}$ are vectors of unknown coefficients, N is the truncated number of the series, and $F_j^u(x), F_j^w(x), F_j^\theta(x)$ are admissible functions satisfying the geometry boundary conditions of the beam. Note that simply supported-simply supported immovable (SS-IM), clamped–clamped immovable (CC-IM), clamped-simply supported immovable (CS-IM), and clamped-free (CF) are considered in the current study. The admissible functions for the several boundary conditions of the beam are provided in Table 1.

By substituting Eq. (17) into Eq. (16), then applying Lagrange's equation as follows (Şimşek 2010b; Wang et al. 2019):

$$\frac{\partial \Pi}{\partial Q_{ij}} - \frac{d}{dt}\left(\frac{\partial \Pi}{\partial \dot{Q}_{ij}}\right) = 0; \quad i = 1,2,3; \quad j = 1,2,3,\cdots,N \tag{18}$$

The governing equation of the FGPM beam can be obtained in the matrix form:

$$\left(\boldsymbol{K}_L + \boldsymbol{K}_{NL} - Mv_M^2\boldsymbol{R}\right)\boldsymbol{Q} + 2Mv_M\boldsymbol{H}\dot{\boldsymbol{Q}} + (\boldsymbol{M} + M\boldsymbol{S})\ddot{\boldsymbol{Q}} = \boldsymbol{F} \tag{19}$$

where $\boldsymbol{K}_L, \boldsymbol{K}_{NL}$ the linear and nonlinear stiffness matrixes of the beam, $\boldsymbol{M}$ is the mass matrix, $\boldsymbol{F}$ is the external load vector. In addition, $M\boldsymbol{S}$, $2Mv_M\boldsymbol{H}$, and $-Mv_M^2\boldsymbol{R}$ represent the influences of the inertia, the Coriolis force, and the centrifugal force of the moving mass. Entries of elements of the matrices are given in detail below.

$$\boldsymbol{K}_L = \begin{bmatrix} \boldsymbol{K}_L^{uu} & \boldsymbol{K}_L^{uw} & \boldsymbol{K}_L^{u\theta} \\ \boldsymbol{K}_L^{wu} & \boldsymbol{K}_L^{ww} & \boldsymbol{K}_L^{w\theta} \\ \boldsymbol{K}_L^{\theta u} & \boldsymbol{K}_L^{\theta w} & \boldsymbol{K}_L^{\theta\theta} \end{bmatrix};$$

$$K_{Lkj}^{uu} = \int_0^L A_{11}F_{k,x}^u(x)F_{j,x}^u(x)bdx;$$

$$K_{Lkj}^{uw} = \int_0^L D_{11b}F_{k,x}^u(x)F_{j,xx}^w(x)bdx;$$

$$K_{Lkj}^{u\theta} = \int_0^L D_{11a}F_{k,x}^u(x)F_{j,x}^\theta(x)bdx;$$

$$K_{Lkj}^{wu} = \int_0^L D_{11b}F_{k,xx}^w(x)F_{j,x}^u(x)bdx;$$

$$K_{Lkj}^{ww} = \int_0^L \left[G_{11b}F_{k,xx}^w(x)F_{j,xx}^w(x) + \left(F_{55} + K_P\right)F_{k,x}^w(x)F_{j,x}^w(x) + K_W F_k^w(x)F_j^w(x)\right]bdx;$$

$$K_{Lkj}^{w\theta} = \int_0^L \left[G_{11c}F_{k,xx}^w(x)F_{j,x}^\theta(x) + F_{55}F_{k,x}^w(x)F_j^\theta(x)\right]bdx;$$

$$K_{Lkj}^{\theta u} = \int_0^L D_{11a}F_{k,x}^\theta(x)F_{j,x}^u(x)bdx;$$

$$K_{Lkj}^{\theta w} = \int_0^L \left[G_{11c}F_{k,x}^\theta(x)F_{j,xx}^w(x) + F_{55}F_k^\theta(x)F_{j,x}^w(x)\right]bdx;$$

$$K_{Lkj}^{\theta\theta} = \int_0^L \left[G_{11a}F_{k,x}^\theta(x)F_{j,x}^\theta(x) + F_{55}F_k^\theta(x)F_j^\theta(x)\right]bdx;$$

$$\boldsymbol{K}_{NL} = \begin{bmatrix} \boldsymbol{0} & \boldsymbol{K}_{NL}^{uw} & \boldsymbol{0} \\ \boldsymbol{K}_{NLkj}^{wu} & \boldsymbol{K}_{NL}^{ww} & \boldsymbol{K}_{NL}^{w\theta} \\ \boldsymbol{0} & \boldsymbol{K}_{NL}^{\theta w} & \boldsymbol{0} \end{bmatrix};$$

$$K_{NLkj}^{uw} = \frac{1}{2}\int_0^L A_{11}\left(\sum_{r=1}^{N} Q_{2r}(t)F_{r,x}^{w}(x)\right)F_{k,x}^{u}(x)F_{j,x}^{w}(x)bdx;$$

$$K_{NLkj}^{wu} = \frac{1}{2}\int_0^L A_{11}\left(\sum_{r=1}^{N} Q_{2r}(t)F_{r,x}^{w}(x)\right)F_{k,x}^{w}(x)F_{j,x}^{u}(x)bdx;$$

$$K_{NLkj}^{ww} = \frac{1}{2}\int_0^L \begin{bmatrix} A_{11}\left(\sum_{r=1}^{N} Q_{2r}(t)F_{r,x}^{w}(x)\right)^2 F_{k,x}^{w}(x)F_{j,x}^{w}(x) \\ +A_{11}\left(\sum_{r=1}^{N} Q_{1r}(t)F_{r,x}^{u}(x)\right)F_{k,x}^{w}(x)F_{j,x}^{w}(x) \\ +D_{11a}\left(\sum_{r=1}^{N} Q_{3r}(t)F_{r,x}^{\theta}(x)\right)F_{k,x}^{w}(x)F_{j,x}^{w}(x) \\ +D_{11b}\left(\sum_{r=1}^{N} Q_{2r}(t)F_{r,x}^{w}(x)\right)F_{k,xx}^{w}(x)F_{j,x}^{w}(x) \\ +D_{11b}\left(\sum_{r=1}^{N} Q_{2r}(t)F_{r,xx}^{w}(x)\right)F_{k,x}^{w}(x)F_{j,x}^{w}(x) \\ +D_{11b}\left(\sum_{r=1}^{N} Q_{2r}(t)F_{r,x}^{w}(x)\right)F_{k,x}^{w}(x)F_{j,xx}^{w}(x) \end{bmatrix} bdx;$$

$$K_{NLkj}^{w\theta} = \frac{1}{2}\int_0^L D_{11a}\left(\sum_{r=1}^{N} Q_{2r}(t)F_{r,x}^{w}(x)\right)F_{k,x}^{w}(x)F_{j,x}^{\theta}(x)bdx;$$

$$K_{NLkj}^{\theta w} = \frac{1}{2}\int_0^L D_{11a}\left(\sum_{r=1}^{N} Q_{2r}(t)F_{r,x}^{w}(x)\right)F_{k,x}^{\theta}(x)F_{j,x}^{w}(x)bdx;$$

$$\boldsymbol{M} = \begin{bmatrix} \boldsymbol{M}^{uu} & \boldsymbol{M}^{uw} & \boldsymbol{M}^{u\theta} \\ \boldsymbol{M}^{wu} & \boldsymbol{M}^{ww} & \boldsymbol{M}^{w\theta} \\ \boldsymbol{M}^{\theta u} & \boldsymbol{M}^{\theta w} & \boldsymbol{M}^{\theta\theta} \end{bmatrix};$$

$$M_{kj}^{uu} = \int_0^L I_A F_k^u(x)F_j^u(x)bdx;$$

$$M_{kj}^{uw} = \int_0^L I_{Db} F_k^u(x)F_{j,x}^w(x)bdx;$$

$$M_{kj}^{u\theta} = \int_0^L I_{Da} F_k^u(x)F_j^{\theta}(x)bdx;$$

$$M_{kj}^{wu} = \int_0^L I_{Db} F_{k,x}^w(x)F_j^u(x)bdx;$$

$$M_{kj}^{ww} = \int_0^L \left[I_A F_k^w(x)F_j^w(x) + I_{Gb} F_{k,x}^w(x)F_{j,x}^w(x)\right]bdx;$$

$$M_{kj}^{w\theta} = \int_0^L I_{Gc} F_{k,x}^w(x)F_j^{\theta}(x)bdx;$$

$$M_{kj}^{\theta u} = \int_0^L I_{Da} F_k^{\theta}(x)F_j^u(x)bdx;$$

$$M_{kj}^{\theta w} = \int_0^L I_{Gc} F_k^{\theta}(x)F_{j,x}^w(x)bdx;$$

$$M_{kj}^{\theta\theta} = \int_0^L I_{Ga} F_k^{\theta}(x)F_j^{\theta}(x)bdx;$$

$$\boldsymbol{R} = \begin{bmatrix} \boldsymbol{0} & \boldsymbol{0} & \boldsymbol{0} \\ \boldsymbol{0} & \boldsymbol{R}^{ww} & \boldsymbol{0} \\ \boldsymbol{0} & \boldsymbol{0} & \boldsymbol{0} \end{bmatrix}; \boldsymbol{S} = \begin{bmatrix} \boldsymbol{S}^{uu} & \boldsymbol{0} & \boldsymbol{0} \\ \boldsymbol{0} & \boldsymbol{S}^{ww} & \boldsymbol{0} \\ \boldsymbol{0} & \boldsymbol{0} & \boldsymbol{0} \end{bmatrix};$$

$$\boldsymbol{H} = \begin{bmatrix} \boldsymbol{H}^{uu} & \boldsymbol{0} & \boldsymbol{0} \\ \boldsymbol{0} & \boldsymbol{H}^{ww} & \boldsymbol{0} \\ \boldsymbol{0} & \boldsymbol{0} & \boldsymbol{0} \end{bmatrix}; \boldsymbol{F} = \begin{Bmatrix} \boldsymbol{0} \\ \boldsymbol{F}^{w} \\ \boldsymbol{0} \end{Bmatrix}$$

$$R_{kj}^{ww} = c(t)\left(F_{k,x}^w F_{j,x}^w\right)\Big|_{x=x_M};$$

$$S_{kj}^{uu} = c(t)\left(F_k^u F_j^u\right)\Big|_{x=x_M};$$

$$S_{kj}^{ww} = c(t)\left(F_k^w F_j^w\right)\Big|_{x=x_M};$$

$$H_{kj}^{ww} = \frac{1}{2}c(t)\left(F_k^w F_{j,x}^w - F_{k,x}^w F_j^w\right)\Big|_{x=x_M}; F_k^w = -c(t)\left(MgF_k^w\right)\Big|_{x=x_M}$$

Note that the numerical results for the dynamic response of the FGPM beam can be obtained by solving Eq. (19), where the fourth-order Runge–Kutta scheme with the initial condition $Q_{ij}(0) = 0$ and $\dot{Q}_{ij}(0) = 0$, is used. A brief description of the fourth-order Runge–Kutta scheme for solving Eq. (19) is as follows:

Table 2 The normalized fundamental frequency $\overline{\omega}$ of the SS-IM FGPM beam with different truncated numbers

e_0	$N=3$	$N=4$	$N=5$	$N=6$	$N=7$	$N=8$	$N=9$
0	3.1432	2.8377	2.8377	2.8369	2.8369	2.8369	2.8369
0.3	3.1321	2.8288	2.8288	2.8280	2.8280	2.8280	2.8280
0.5	3.1473	2.8438	2.8438	2.8430	2.8430	2.8430	2.8430
0.8	3.2721	2.9610	2.9609	2.9601	2.9601	2.9601	2.9601

Table 3 The normalized fundamental frequencies of SS-IM isotropic beams

K_0	Model	J_0/π^2			
		0	0.5	1	2.5
$L/h=15$					
0	Chen et al. (2004)	3.1302	3.4667	3.7266	4.2881
	Present	3.1299	3.4671	3.7274	4.2897
10^2	Chen et al. (2004)	3.7389	3.9517	4.1347	4.5735
	Present	3.7398	3.9529	4.1361	4.5755
$L/h=5$					
0	Chen et al. (2004)	3.048	3.3946	3.658	4.2183
	Present	3.0454	3.3987	3.6671	4.2395
10^2	Chen et al. (2004)	3.6705	3.884	4.0664	4.4991
	Present	3.6798	3.8976	4.0839	4.5279

Table 4 The normalized fundamental frequencies of CC-IM isotropic beams

K_0	Model	J_0/π^2			
		0	0.5	1	2.5
$L/h=15$					
0	Chen et al. (2004)	4.6655	4.8039	4.9303	5.2567
	Present	4.6615	4.8014	4.9291	5.2586
10^2	Chen et al. (2004)	4.8927	5.0135	5.1254	5.4198
	Present	4.8900	5.0121	5.1250	5.4220
$L/h=5$					
0	Chen et al. (2004)	4.2634	4.4197	4.5595	4.9102
	Present	4.2584	4.4242	4.5716	4.9395
10^2	Chen et al. (2004)	4.5418	4.6721	4.791	5.0974
	Present	4.5458	4.6839	4.8094	5.1319

Step 1: Set $y(t) = \begin{Bmatrix} Q(t) \\ \dot{Q}(t) \end{Bmatrix}$ and $\dot{y}(t) = \begin{Bmatrix} \dot{Q}(t) \\ \ddot{Q}(t) \end{Bmatrix}$,

where $\boldsymbol{Q}(t) = \left\{ Q_{11}(t)\, Q_{12}(t) \ldots Q_{31}(t)\, Q_{32}(t) \ldots Q_{3N}(t) \right\}^T$.

Step 2: Rewrite Eq. (19) in the form: $\dot{y} = Ay(t) + y_*(t) = f(y, t)$,

where

$$\boldsymbol{A} = \begin{bmatrix} \boldsymbol{0} & \boldsymbol{I} \\ -(\boldsymbol{M}+\boldsymbol{MS})^{-1}\left(\boldsymbol{K}^L + \boldsymbol{K}^{NL}(\boldsymbol{Q}) - Mv_M^2\boldsymbol{R}\right) & -2Mv_M(\boldsymbol{M}+\boldsymbol{MS})^{-1}\boldsymbol{H} \end{bmatrix}$$

Table 5 The normalized fundamental frequency of FGPM beams

Boundary conditions	Model	e_0			
		0.2	0.4	0.6	0.8
T1 – *Uniform distribution*					
CC-IM	Nguyen et al. (2022b)	0.306	0.293	0.277	0.255
	Present	0.3060	0.2932	0.2773	0.2551
CS-IM	Nguyen et al. (2022b)	0.213	0.204	0.193	0.177
	Present	0.2126	0.2037	0.1926	0.1772
SS-IM	Nguyen et al. (2022b)	0.137	0.131	0.124	0.114
	Present	0.1369	0.1312	0.1241	0.1141
CF	Nguyen et al. (2022b)	0.049	0.047	0.044	0.041
	Present	0.0489	0.0469	0.0443	0.0408
T2 – *Symmetric distribution*					
CC-IM	Nguyen et al. (2022b)	0.315	0.315	0.318	0.326
	Present	0.3154	0.3152	0.3175	0.3260
CS-IM	Nguyen et al. (2022b)	0.220	0.220	0.222	0.229
	Present	0.2193	0.2194	0.2214	0.2282
SS-IM	Nguyen et al. (2022b)	0.141	0.142	0.143	0.148
	Present	0.1413	0.1415	0.1431	0.1479
CF	Nguyen et al. (2022b)	0.050	0.051	0.051	0.053
	Present	0.0505	0.0506	0.0511	0.0529

$$y_*(t) = \begin{Bmatrix} \boldsymbol{0} \\ (\boldsymbol{M}+\boldsymbol{MS})^{-1}\boldsymbol{F}(t) \end{Bmatrix}$$

Step 3: Apply the fourth-order Runge-Kutta method as follows:

$$\boldsymbol{y}_{k+1} = \boldsymbol{y}_k + \frac{1}{6}\left(\boldsymbol{R}_{1k} + 2\boldsymbol{R}_{2k} + 2\boldsymbol{R}_{3k} + \boldsymbol{R}_{4k}\right)$$

with the initial condition: $\boldsymbol{y}_0 = \boldsymbol{y}(t)|_{t=0} = \begin{Bmatrix} \boldsymbol{Q}(t) \\ \dot{\boldsymbol{Q}}(t) \end{Bmatrix}\Bigg|_{t=0} = \begin{Bmatrix} \boldsymbol{0} \\ \boldsymbol{0} \end{Bmatrix}$.

where

$$\boldsymbol{R}_{1k} = \Delta t.f\left(t_k, \boldsymbol{y}_k\right); \boldsymbol{R}_{2k} = \Delta t.f\left(t_k + \frac{\Delta t}{2}, \boldsymbol{y}_k + \frac{\boldsymbol{R}_1}{2}\right);$$
$$\boldsymbol{R}_{3k} = \Delta t.f\left(t_k + \frac{\Delta t}{2}, \boldsymbol{y}_k + \frac{\boldsymbol{R}_2}{2}\right); \boldsymbol{R}_{4k} = \Delta t.f\left(t_k + \Delta t, \boldsymbol{y}_k + \boldsymbol{R}_3\right);$$

$\boldsymbol{y}_k, \boldsymbol{y}_{k+1}$ are at values of $\boldsymbol{y}(t)$ at the time t_k and t_{k+1}; and Δt is the time step ($t_{k+1} = t_k + \Delta t$).

Step 4: When the results ($\boldsymbol{y}_0, \boldsymbol{y}_1 \ldots, \boldsymbol{y}_n$) of any time step are determined, the displacement field of the beam at any time step can be obtained.

For linear free-vibration problems, the coefficient vector can be assumed to be in the form as $\boldsymbol{Q} = \boldsymbol{Q}_0 e^{i\omega t}$. The external load vector ($\boldsymbol{F}$), the moving mass M, and the nonlinear terms are ignored in Eq. (19). By substituting $\boldsymbol{Q} = \boldsymbol{Q}_0 e^{i\omega t}$ into the resulting equation, yields:

$$\left(\boldsymbol{K}_L - \boldsymbol{M}\omega^2\right)\boldsymbol{Q}_0 = \boldsymbol{0} \tag{20}$$

Note that the natural angular frequencies and vibration modes of the FGPM beam can be determined by solving Eq. (20).

If the mass moves along the beam, instantaneous mass and stiffness matrices must be employed to solve for the instantaneous natural frequencies of the complete system (beam and moving mass) (Esen 2017). In this case, the natural frequency of the system ω_s can be determined from the following equation:

$$\left(\boldsymbol{K}_s - \boldsymbol{M}_s\omega_s^2\right)\boldsymbol{Q}_0 = \boldsymbol{0} \tag{21}$$

in which: $\boldsymbol{K}_s(t) = \boldsymbol{K}_L - M v_M^2 \boldsymbol{R}(t); \quad \boldsymbol{M}_s = \boldsymbol{M} + M\boldsymbol{S}(t)$.

5 Numerical Results and Discussions

The proposed model is verified for the free vibration and dynamic features of the FGPM beam with the elastic foundation under the moving mass via three numerical examples. Parametric studies are then performed to investigate the free vibration and nonlinear dynamic features of the FGPM beam with the Winkler-Pasternak foundation under the traveling mass.

Otherwise stated, the adopted material properties for FGPM (the metal foam) are $\rho_1 = 7850$ kg/m^3, $E_1 = 200$ GPa, $\nu = 1/3$ (Chen et al. 2016). For convenience, the normalized parameters (i.e., normalized deflection $\overline{w}(t)$, mass ratio m_r, natural angular frequency $\overline{\omega}$, elastic foundation parameters K_0, J_0, and time variable t^*) are adopted in the present study as follows (Chen et al. 2016; Ait Atmane et al. 2017; Thai and Vo 2012):

$$\begin{gathered}\overline{w}(t) = \frac{w_0(L/2,t)}{w^*}; m_r = \frac{M}{I_A L}; \overline{\omega} = \omega\frac{L^2}{h}\sqrt{\frac{\rho_1}{E_1}};\\ K_0 = K_W\frac{L^4}{E_1 I}; J_0 = K_P\frac{L^2}{E_1 I}; t^* = \frac{v_0 t}{L};\end{gathered} \tag{22}$$

in which, w^* is the maximum deflection of the simply supported beam due to a concentrated load $P = Mg$ applied at the beam midspan, and I is the area moment of inertia for the rectangular section of the beam; they can be defined by

$$w^* = \frac{MgL^3}{48E_1 I}; I = \frac{bh^3}{12} \tag{23}$$

5.1 Convergence Study

In this subsection, a convergence study is conducted for the Ritz solution of the beam problem. The FGPM beam subjected to the SS-IM boundary condition, with symmetric material distribution, and parameters $L/h = 20$, $K_0 = J_0 = 0$, is considered here. The normalized frequency ($\overline{\omega}$) of the beam with different truncated numbers, N, and porosity coefficient, e_0, are listed in Table 2. We can see that the results almost converge when $N \geq 6$; thus, to ensure the convergence, the truncated number $N = 9$ is chosen for further investigations.

5.2 Verification Examples

For verifications, the first example is for the free vibration of an isotropic beam resting on an elastic foundation; the second is for the free vibration of an FGPM beam without an elastic foundation; and the last is for the dynamic response of isotropic beams under the traveling mass.

Example 1. Free vibration of isotropic beams resting on the elastic foundation

In this example, an isotropic beam resting on a Pasternak elastic foundation with the material parameters $\rho = \rho_1 = 7850$ kg/m^3, $E = E_1 = 200$ GPa, $\nu = 0.3$, is evaluated. The present results ($N = 9$) of the beam are verified with those of Chen et al. (2004), who used a mixed technique between the differential quadrature and state space methods. The normalized fundamental frequencies $\tilde{\omega} = \sqrt{\omega\left(\rho A L^4/(EI)\right)^{1/4}}$ of the beam with the SS-IM and CC-IM boundary conditions are listed in Tables 3 and 4. Two cases of the length-to-thickness ratios considered here are $L/h = 15$ and 5. We can see that

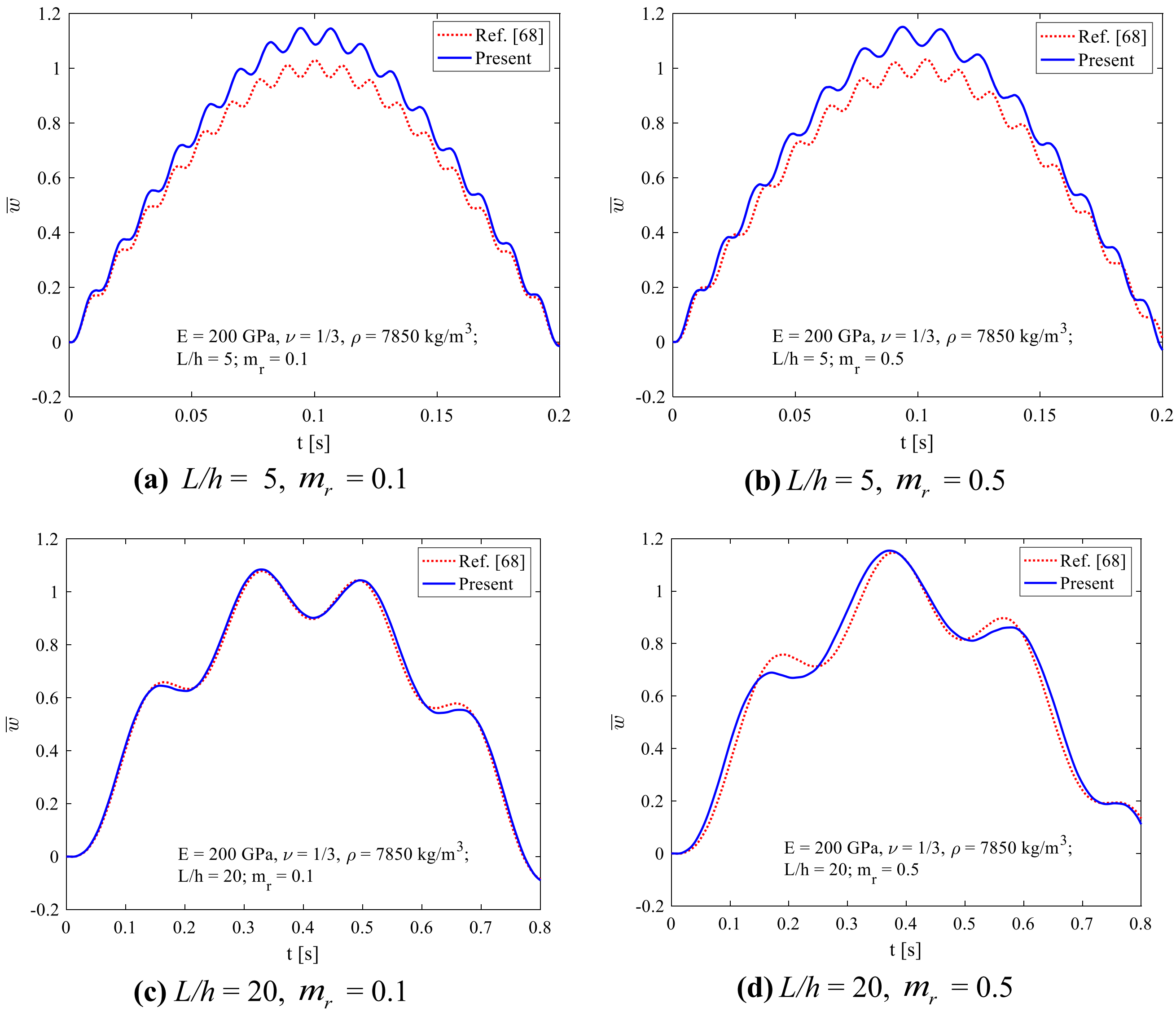

Fig. 3 Verification of dynamic response of isotropic beams under the moving mass

the current results are consistent with those of Chen et al. (2004) for all cases investigated.

Example 2. Free vibration of FGPM beams

An FGPM beam with the material properties (metal foam) $\rho_1 = 7850$ kg/m^3, $E_1 = 200$ GPa, $\nu = 1/3$, and the length-to-thickness ratio $L/h = 20$ is considered here. The normalized fundamental frequencies, $\hat{\omega} = \omega L\sqrt{\rho_1\left(1-\nu^2\right)/E_1}$, of the FGPM beam with different porosity coefficients e_0 and boundary conditions are compared in Table 5. The findings show that the fundamental frequencies from the present model agree well with those of Nguyen et al. (2022b) (both T1 and T2 patterns), who used the Ritz procedure and improved high-order shear deformation beam theory.

Example 3. Dynamic response of isotropic beams under a moving mass

Consider a simply supported isotropic beam with the material properties $\rho = \rho_1 = 7850$ kg/m^3, $E = E_1 = 200$ GPa, $\nu = 1/3$. The linear dynamic responses of the beam for two cases of length-to-thickness ratio ($L/h = 5$, 20) and two cases of mass ratio ($m_r = 0.1$, 0.5) are investigated and plotted in Fig. 3. These results, with the number of terms $N = 9$, are compared with the formula of Stanišić and Hardin (1969) using Euler–Bernoulli beam theory, as follows:

$$w_0(x,t) = \frac{2P}{L}\sum_{m=1}^{\infty}\Phi_m(x)q_m(t) \tag{24}$$

where

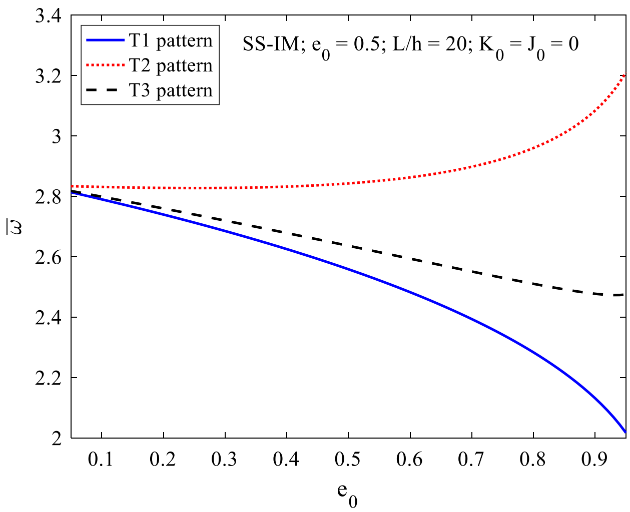

Fig. 4 Effect of the porosity coefficient on the frequency of the beam

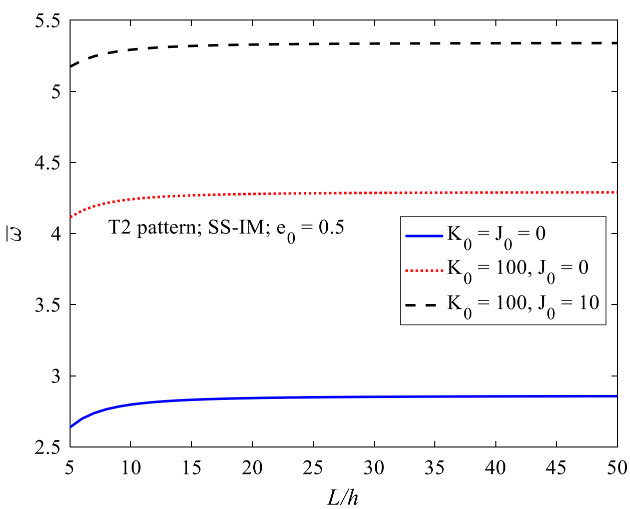

Fig. 5 Effects of the elastic foundation parameters and length-to-thickness ratio on the frequency of the beam

$$\Phi_m(x) = \sin\frac{m\pi x}{L}; \quad q_m(t) = \frac{1}{\omega_m^2\left(1-\lambda_m^2\right)}\left(\sin\frac{m\pi v_M t}{L} - \lambda_m \sin\frac{\omega_m}{\sqrt{1+R}}t\right);$$

$$\lambda_m = \frac{m\pi v_M\sqrt{1+R}}{L\omega_m}; \quad \omega_m = \frac{m^2\pi^2}{L^2}\sqrt{\frac{EI}{\mu}}; \quad P = \frac{Mg}{\mu}; \quad R = \frac{M}{\mu L}; \quad \mu = \rho A; \quad A = bh.$$

The findings show that in the case of the long beam ($L/h = 20$) and the mass ratio $m_r = 0.1$, the deflection-time curves of the two approaches almost coincided, as shown in Fig. 3c. Particularly, the midspan deflection of the beam is $\overline{w}_{\max} = 1.0847$, and the difference between the present result

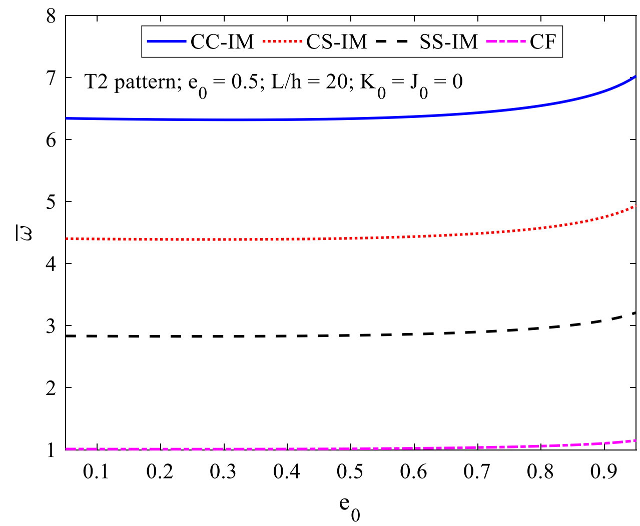

Fig. 6 Effect of various boundary conditions on the frequency of the beam

and that of Stanišić and Hardin (1969) is around 0.57%. Note that the Reddy's beam theory is used in the present study, while the classical beam theory was used in the work of Stanišić and Hardin (1969) (i.e., Eq. (24)). Besides, the effects of Coriolis force and centripetal force were also not included in their simulation. Thus, for the short beam ($L/h = 5$) the bigger discrepancies between obtained results as shown in Fig. 3a and b are obvious.

From the three verification examples above, we can see that the theoretical formulations and the proposed solution are highly reliable, and they can be used for further investigations.

5.3 Free Vibration Analysis

Effects of the porosity distributions and porosity coefficient on the normalized fundamental frequency of the FGPM beam ($e_0 = 0.5$, $L/h = 20$, $K_0 = J_0 = 0$) under the SS-IM boundary condition are shown in Fig. 4. We can see that, for two patterns of porosity distributions (T1 and T3), when increasing the coefficient e_0, the frequencies of the FGPM beam decrease gradually. In contrast, for symmetric distribution (T2 pattern), the frequency of the FGPM beam increases with respect to the porosity coefficient. The reason for the different variation trend of normalized

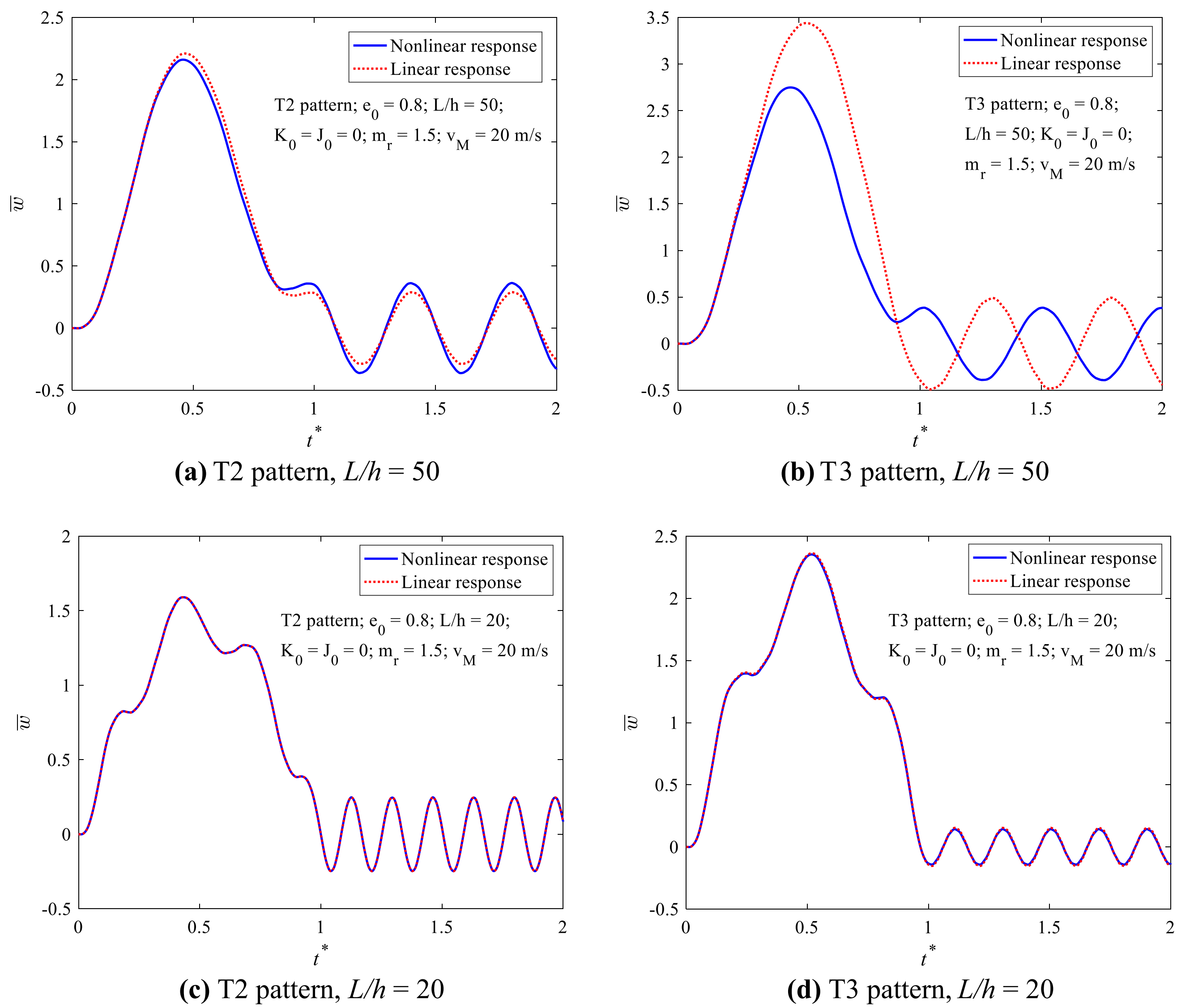

Fig. 7 Effect of geometric nonlinearity on the deflection-time curve of FGPM beam

fundamental frequency is due to the relative correlation between the beam stiffness effect and cross-sectional inertia effect as the porosity coefficient increases. For the T2 pattern, the rate of reduction in beam stiffness is smaller than that of the cross-sectional inertia. Thus, it can be said that the beam with the symmetric distribution (T2 pattern) is the most effective in the bending stiffness than other patterns (T1 and T3).

The effect of the elastic foundation parameters (K_0, J_0) and the length-to-thickness ratio (*L/h*) on the normalized fundamental frequency of the FGPM beam (T2—symmetric pattern, $e_0 = 0.5$) with SS-IM boundary condition is shown in Fig. 5. It can be noticed that, for each *L/h* ratio, the beam with the Pasternak foundation ($K_0 = 100$, $J_0 = 10$) always has the highest frequency, then the beam with the Winkler foundation ($K_0 = 100$, $J_0 = 0$), and the FGPM beam without the elastic foundation ($K_0 = J_0 = 0$) has the lowest frequency. Note that the increase in elastic foundation coefficients contributes to an increase in the overall stiffness of the beam structure. In addition, regarding the effect of the geometric parameter, the results show that the variation in the frequency of the beam is insignificant when $L/h > 15$.

The effect of various boundary conditions (CC-IM, CS-IM, SS-IM, CF) on the frequency of the FGPM beam (T2—symmetric pattern, $e_0 = 0.5$, $L/h = 20$, $K_0 = J_0 = 0$) is shown in Fig. 6. The results show that the CC-IM beam always has the highest frequency, followed by the CS-IM, SS-IM, and CF beams.

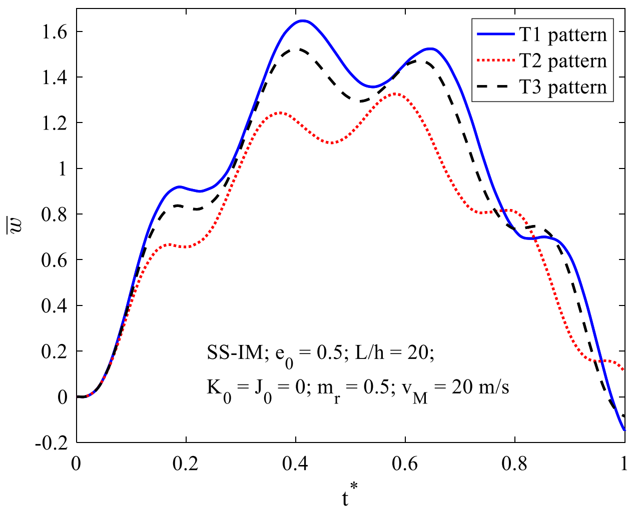

Fig. 8 Effect of the porosity distribution on the deflection-time curve of the FGPM beam

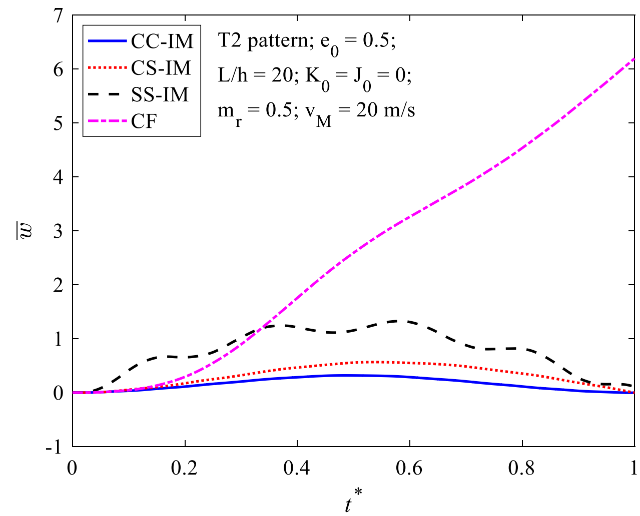

Fig. 10 Effect of boundary conditions on the deflection-time curve of the beam

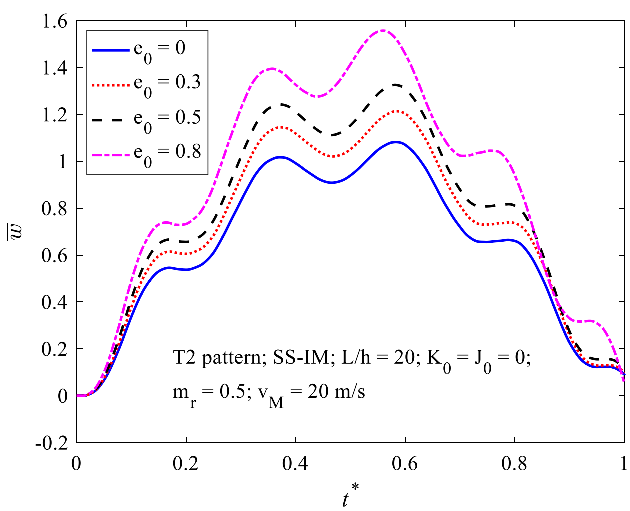

Fig. 9 Effect of the porosity coefficient on the deflection-time curve of the FGPM beam

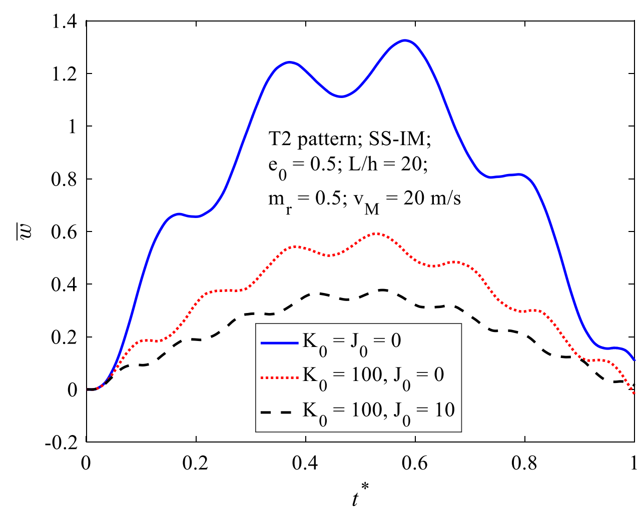

Fig. 11 Effect of the elastic foundation parameters on the deflection-time curve of the beam

5.4 Linear and Nonlinear Dynamic Responses of FGPM Beams

The nonlinear behaviors of the beam depend on many factors, such as geometric parameters, loadings, boundary conditions, material, etc. In the present work, the geometric nonlinearity in the von Kármán sense is considered. In this section, the linear and nonlinear dynamic responses of the FGPM beam are compared for different geometric parameters (*L/h*) and two patterns of porosity distributions (symmetric-T2 and asymmetric-T3). Nonlinear and linear responses of the midspan deflection, $\overline{w}$, of the FGPM beam with the SS-IM boundary condition are presented in Fig. 7. It can be observed that, for the long beam ($L/h = 50$), the linear beam gives significantly greater deflections than the results of the nonlinear beam, especially for the beam with the T3 pattern, as shown in Fig. 7b. It is clear that the influence of the geometric nonlinearity on the dynamic responses of the FGPM beam (the difference between the linear and nonlinear cases) is significant for the T3 pattern (asymmetric distribution), but is insignificant for the T2 pattern (symmetric distribution).

The nonlinear dynamic responses of the SS-IM FGPM beam with different kinds of porosity distributions (T1-uniform, T2-symmetric, and T3-asymmetric patterns) are compared and plotted in Fig. 8 ($e_0 = 0.5$, $L/h = 20$, $m_r = 0.5$,

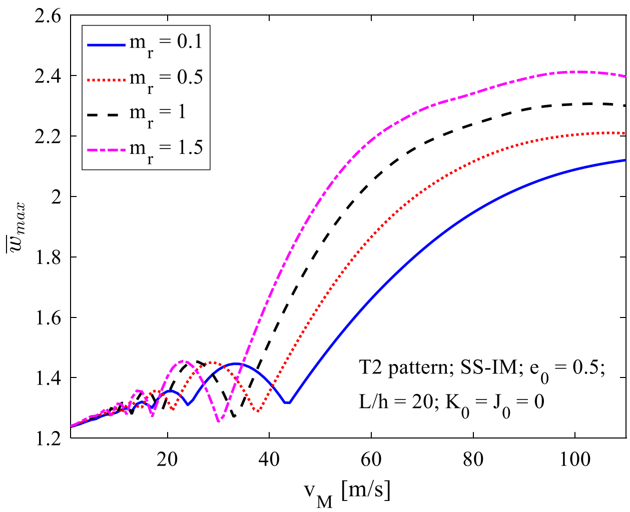

Fig. 12 Effect of the moving mass velocity on the dynamic response of the FGPM beam with different mass ratios

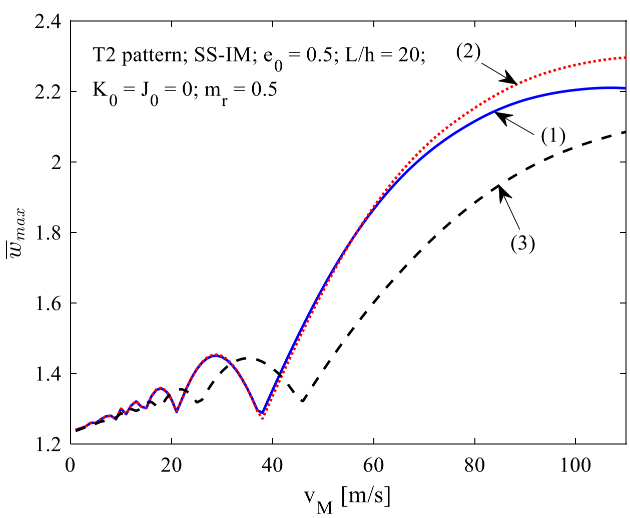

Fig. 13 A comparison of the FGPM beam under (1) a moving mass with Coriolis and centrifugal effects, (2) a moving mass without Coriolis and centrifugal effects, and (3) a moving load

$v_M = 20$ m/s). The findings show that, with the same porosity coefficient, the symmetric distribution (T2) often has the smallest deflection. This is because the rate of reduction in the beam stiffness of the symmetric distribution pattern (T2) is smaller than the remaining two distribution patterns as above-mentioned. Similarly, the dynamic responses of the SS-IM FGPM beam with different porosity coefficients are compared and plotted in Fig. 9 (T2 pattern, $L/h = 20$, $m_r = 0.5$, $v_M = 20$ m/s). The findings show that when the porosity coefficient rises, the midspan deflection of the beam increases (the stiffness of the beam decreases).

Next, the effect of boundary conditions (CC-IM, SC-IM, SS-IM, and CF) on the dynamic response of the FGPM beam (T2 pattern) is compared in Fig. 10 ($e_0 = 0.5$, $L/h = 20$, $m_r = 0.5$, $v_M = 20$ m/s). The results of the midspan deflection show that the CF beam has the greatest deflection, followed by the SS-IM, SC-IM, and CC-IM beams. In addition, the effect of elastic foundation parameters on the dynamic response of the FGPM beam (T2 pattern) under the SS-IM boundary condition is shown in Fig. 11. From the results, we can see that the beam without elastic foundations has the greatest deflection, followed by the case of beams on the Winkler foundation and Pasternak foundation.

Figure 12 presents the effect of the moving velocity v_M on the maximum midspan deflection $\overline{w}_{\max}$ of the FGPM beam (symmetricT2 distribution, SS-IM boundary condition); different values of the mass ratio ($m_r = 0.1$, 0.5, 1, 1.5) are considered. In this example, the FGPM beam with the parameters $L/h = 20$, $e_0 = 0.5$,$K_0 = J_0 = 0$, is performed. It can be observed that the mass ratio has a significant influence on the dynamic response of the beam under moving mass, with increases of the moving mass velocity, the variation of the deflection $\overline{w}_{\max}$ is very complicated at the first stage. After v_M reaches a certain value, the maximum midspan deflection $\overline{w}_{\max}$ of the beam increases monotonously, reaches extremes, and then decreases again. In addition, note that when increasing the mass ratio m_r, the maximum value of the midspan deflection of the beam $\overline{w}_{\max}$ increases. This could be because the maximum value of the midspan deflection also depends on the fundamental natural frequency as mentioned by Malekzadeh et al. (2022a; 2022b). For example, at moving velocity $v_M = 80$ m/s, for the cases of the mass ratio m_r (0.1; 0.5; 1; 1.5), normalized maximum mid-span deflections $\overline{w}_{\max}$ are (1.9568; 2.1230; 2.2447; 2.3463), and the corresponding fundamental natural frequencies of the entire system are (327.49 rad/s; 253.35 rad/s; 206.60 rad/s; 178.79 rad/s). Thus, when the mass ratio increases from 0.1 to 0.5, the normalized maximum mid-span deflection increases by 8.5%, and fundamental natural frequency decreases by 22.6%. Also, when the mass ratio $m_r = 1$, the normalized maximum mid-span deflection increases by 14.7%, and fundamental natural frequency decrease by 36.9%. This can be explained by the increase in the mass ratio affecting the total mass and stiffness matrices of the entire system as described in Eqs. (19) and (21).

Figure 13 compares the responses of the FGPM beam ($e_0 = 0.5$, T2 pattern, the SS-IM boundary condition) subjected to a moving mass with and without Coriolis and centrifugal effects, and a moving load. Relationships between the maximum midspan deflection ($\overline{w}_{\max}$) of the beam and the moving velocity v_M are illustrated here in different approaches, including (1) a moving mass with Coriolis and centrifugal effects, (2) a moving mass without Coriolis and centrifugal effects, and (3) a moving load considered.

It can be seen that the maximum deflections of the beam with the moving load (i.e., case (3)) are smaller than those of the beam with the moving mass (i.e., cases (1) and (2)). Note that the kinetic energy of the mass of moving mass is ignored when the moving load model is considered, while it is included when the moving mass model is used. The difference between the cases with and without the Coriolis and centrifugal effects is significant when the velocity of the moving mass increases.

6 Conclusions

This paper provides solutions for the nonlinear dynamic features of beams with a Winkler-Pasternak foundation under a traveling mass. The beam is made from a functionally graded porous material (FGPM), and three patterns of porosity distributions are considered, including symmetric, asymmetric, and uniform distributions. The governing system of equations is developed using Lagrange's equation, the Ritz procedure, and Reddy's beam theory. Nonlinear dynamic features of the FGPM beam under the moving mass are then computed using the Runge–Kutta scheme. Influences of various parameters on the dynamic features of the FGPM beam under the traveling mass are studied via numerical results. The key conclusions of the study can be briefly summarised here:

- The results show that the FGPM beam with the symmetric distribution (T2 pattern) is more effective than other patterns (T1 and T3). Regarding the geometric parameter, when the length-to-thickness ratio $L/h > 15$, the variation in the frequency of the beam is insignificant.
- The influence of the geometric nonlinearity on the dynamic responses of the FGPM beam is significant for the T3 pattern (asymmetric distribution) but is insignificant for the T2 pattern (symmetric distribution).
- The maximum deflections of the beam with the moving load are smaller than those of the beam with the moving mass. Besides, the difference between the cases with and without the Coriolis and centrifugal effects is significant when increasing the velocity of the moving mass.
- As expected, the midspan deflections of the CF beam have the highest values, followed by the SS, SC, and CC beams. Lastly, the stiffness of the FGPM beam structure increases when the foundation coefficients are increased.

Acknowledgements This research is funded by Ministry of Education and Training under grand number B2023-XDA-10.

References

Ait Atmane H, Tounsi A, Bernard F (2017) Effect of thickness stretching and porosity on mechanical response of a functionally graded beams resting on elastic foundations. Int J Mech Mater Design 13:71–84

Akbaş ŞD, Dastjerdi S, Akgöz B, Civalek Ö (2022) Dynamic analysis of functionally graded porous microbeams under moving load. Transp Porous Med 142:209–227. https://doi.org/10.1007/s11242-021-01686-z

Akin JE, Mofid M (1989) Numerical solution for response of beams with moving mass. J Struct Eng 115(1):120–131

Alimoradzadeh M, Akbas S (2022) Nonlinear dynamic behavior of functionally graded beams resting on nonlinear viscoelastic foundation under moving mass in thermal environment. Struct Eng Mech 81(6):705–714

Ashby MF, Evans T, Fleck NA, Hutchinson J, Wadley H, Gibson L (2000) Metal foams: a design guide. Elsevier, USA

Badiche X, Forest S, Guibert T, Bienvenu Y, Bartout JD, Ienny P, Croset M, Bernet H (2000) Mechanical properties and non-homogeneous deformation of open-cell nickel foams: application of the mechanics of cellular solids and of porous materials. Mater Sci Eng, A 289(1):276–288

Bagheri H, Kiani Y, Eslami MR (2023) Geometrically nonlinear response of FGM beams on elastic foundation subjected to thermal shock. Iran J Sci Technol, Trans Mech Eng 47(1):187–201

Bahranifard F (2020) MR Golbahar Haghighi, P Malekzadeh, In-plane responses of multilayer FG-GPLRC curved beams in thermal environment under moving load. Acta Mech 231(7):2679–2696

Bahranifard F, Malekzadeh P (2022b) MR Golbahar Haghighi, Moving load response of ring-stiffened sandwich truncated conical shells with GPLRC face sheets and porous core. Thin-Walled Structures 180:109984.

Bahranifard F, Malekzadeh P, Golbahar MR Haghighi (2022a) Large amplitude vibration of sandwich beams with GPLRC face sheets and porous core under moving load. Mech Based Design Struct Mach pp. 1–24. https://doi.org/10.1080/15397734.2022.2156884

Banhart J (2001) Manufacture, characterisation and application of cellular metals and metal foams. Prog Mater Sci 46(6):559–632

Barati MR, Zenkour AM (2017) Investigating post-buckling of geometrically imperfect metal foam nanobeams with symmetric and asymmetric porosity distributions. Compos Struct 182:91–98

Boggarapu V, Gujjala R, Ojha S, Acharya S, Chowdary S, Kumar GD (2021) State of the art in functionally graded materials. Compos Struct 15(262):113596

Chen WQ, Lü CF, Bian ZG (2004) A mixed method for bending and free vibration of beams resting on a Pasternak elastic foundation. Appl Math Model 28(10):877–890

Chen D, Yang J, Kitipornchai S (2016) Free and forced vibrations of shear deformable functionally graded porous beams. Int J Mech Sci 108–109:14–22

Chen J-S, Chen S-Y, Hsu W-Z (2021) Effects of geometric nonlinearity on the response of a long beam on viscoelastic foundation to a moving mass. J Sound Vib 497:115961

Dang X-H, Nguyen V-L, Tran M-T, Nguyen Thi B-P (2022) Free vibration characteristics of rotating functionally graded porous circular cylindrical shells with different boundary conditions. Iran J Sci Technol Trans Mech Eng 46(1):167–183

Esen İ (2011) Dynamic response of a beam due to an accelerating moving mass using moving finite element approximation. Math Comput Appl 16(1):171–182. https://doi.org/10.1590/1679-78255102

Esen İ (2013) A new finite element for transverse vibration of rectangular thin plates under a moving mass. Finite Elem Anal Des 66:26–35

Esen İ (2015) A new FEM procedure for transverse and longitudinal vibration analysis of thin rectangular plates subjected to a variable

velocity moving load along an arbitrary trajectory. Latin Am J Solids Struct 12:808–830
Esen I (2017) A modified FEM for transverse and lateral vibration analysis of thin beams under a mass moving with a variable acceleration. Latin Am J Solids Struct 14:485–511
Esen I (2019a) Dynamic response of functional graded Timoshenko beams in a thermal environment subjected to an accelerating load. Eur J Mech A Solids 78:103841
Esen I (2019b) Dynamic response of a functionally graded Timoshenko beam on two-parameter elastic foundations due to a variable velocity moving mass. Int J Mech Sci 153–154:21–35
Esen I (2020a) Dynamics of size-dependant Timoshenko micro beams subjected to moving loads. Int J Mech Sci 175:105501
Esen I (2020b) Response of a micro-capillary system exposed to a moving mass in magnetic field using nonlocal strain gradient theory. Int J Mech Sci 188:105937
Esen I, Koç MA (2015a) Dynamic response of a 120 mm smoothbore tank barrel during horizontal and inclined firing positions. Latin Am J Solids Struct 12:1462–1486
Esen İ, Koç MA (2015b) Optimization of a passive vibration absorber for a barrel using the genetic algorithm. Expert Syst Appl 42(2):894–905
Esen I, Eltaher MA, Abdelrahman AA (2023) Vibration response of symmetric and sigmoid functionally graded beam rested on elastic foundation under moving point mass. Mech Based Des Struct Mach 51(5):2607–2631
Esen I, Koc MA, Cay Y (2018) Finite element formulation and analysis of a functionally graded Timoshenko beam subjected to an accelerating mass including inertial effects of the mass. Latin Am J Solids Struct 15(10):e119. https://doi.org/10.1590/1679-78255102
Foda MA, Abduljabbar Z (1998) A dynamic green function formulation for the response of a beam structure to a moving mass. J Sound Vib 210(3):295–306
Froio D, Rizzi E, Simões FM, Pinto Da Costa A (2018) Dynamics of a beam on a bilinear elastic foundation under harmonic moving load. Acta Mech 229:4141–4165
Fryba L, Frýba L (1999) Vibration of solids and structures under moving loads. Thomas Telford, Prague
Jiang J-Q (2011) Transient responses of Timoshenko beams subject to a moving mass. J Vib Control 17(13):1975–1982
Jorge PC, Simões F, Da Costa AP (2015) Dynamics of beams on non-uniform nonlinear foundations subjected to moving loads. Comput Struct 148:26–34
Kiani K, Nikkhoo A, Mehri B (2009) Prediction capabilities of classical and shear deformable beam models excited by a moving mass. J Sound Vib 320(3):632–648
Koç MA, Esen İ (2017) Modelling and analysis of vehicle-structure-road coupled interaction considering structural flexibility, vehicle parameters and road roughness. J Mech Sci Technol 31(5):2057–2074
Koç MA, Esen İ, Eroğlu M, Çay Y, Çerlek Ö (2018) Dynamic analysis of flexible structures under the influence of moving multiple vehicles. El-Cezeri Fen Ve Mühendislik Dergisi 5(1):176–181
Mamandi A, Kargarnovin MH (2011) Dynamic analysis of an inclined Timoshenko beam traveled by successive moving masses/forces with inclusion of geometric nonlinearities. Acta Mech 218(1–2):9–29
Michaltsos G (2002) Dynamic behaviour of a single-span beam subjected to loads moving with variable speeds. J Sound Vib 258(2):359–372
Moghaddasi M, Kiani Y (2022) Free and forced vibrations of graphene platelets reinforced composite laminated arches subjected to moving load. Meccanica 57(5):1105–1124
Nguyen V-L, Hoang T-P (2019) Analytical solution for free vibration of stiffened functionally graded cylindrical shell structure resting on elastic foundation. Sn Appl Sci 1(10):1150
Nguyen DK, Vu ANT, Pham VN, Truong TT (2022a) Vibration of a three-phase bidirectional functionally graded sandwich beam carrying a moving mass using an enriched beam element. Engineering with Computers 38(Suppl 5):4629–4650
Nguyen N-D, Nguyen T-N, Nguyen T-K, Vo TP (2022b) A new two-variable shear deformation theory for bending, free vibration and buckling analysis of functionally graded porous beams. Compos Struct 282:115095
Nguyen V-L, Tran M-T, Limkatanyu S, Rungamornrat J (2023) Free vibration analysis of rotating FGP sandwich cylindrical shells with metal-foam core layer. Mech Adv Mater Struct 30(16):3318–3331
Nikkhoo A, Rofooei FR, Shadnam MR (2007) Dynamic behavior and modal control of beams under moving mass. J Sound Vib 306(3):712–724
Ouyang H (2011) Moving-load dynamic problems: a tutorial (with a brief overview). Mech Syst Signal Process 25(6):2039–2060
C Özarpa, I Esen, Modelling the dynamics of a nanocapillary system with a moving mass using the non-local strain gradient theory. Math Method Appl Sci n/a(n/a). https://doi.org/10.1002/mma.6812
Phu KV, Bich DH, Doan LX (2022) Nonlinear forced vibration and dynamic buckling analysis for functionally graded cylindrical shells with variable thickness subjected to mechanical load. Iran J Sci Technol, Trans Mech Eng 46(3):649–665
Reddy JN (2003) Mechanics of laminated composite plates and shells: theory and analysis. CRC Press, New York
Samani FS, Pellicano F (2009) Vibration reduction on beams subjected to moving loads using linear and nonlinear dynamic absorbers. J Sound Vib 325(4–5):742–754
Sheng G, Wang X (2017) The geometrically nonlinear dynamic responses of simply supported beams under moving loads. Appl Math Model 48:183–195
Shokouhifard V, Mohebpour S, Malekzadeh P, Golbaharhaghighi M (2020a) Inverse dynamic analysis of an inclined FGM beam due to moving load for estimating the mass of moving load based on a CGM. Iran J Sci Technol, Trans Mech Eng 44(3):543–556
Shokouhifard V, Mohebpour S, Malekzadeh P, Alighanbari H (2020b) An inclined FGM beam under a moving mass considering Coriolis and centrifugal accelerations. Steel Compos Struct 35(1):61–76
Şimşek M (2010a) Non-linear vibration analysis of a functionally graded Timoshenko beam under action of a moving harmonic load. Compos Struct 92(10):2532–2546
Şimşek M (2010b) Vibration analysis of a functionally graded beam under a moving mass by using different beam theories. Compos Struct 92(4):904–917
Şimşek M, Kocatürk T (2009) Free and forced vibration of a functionally graded beam subjected to a concentrated moving harmonic load. Compos Struct 90(4):465–473
Şi̇mşek M, Kocatürk T, (2007) Free vibration analysis of beams by using a third-order shear deformation theory. Sadhana 32(3):167–179
Smith BH, Szyniszewski S, Hajjar JF, Schafer BW, Arwade SR (2012) Steel foam for structures: a review of applications, manufacturing and material properties. J Constr Steel Res 71:1–10
Stanišić MM, Hardin JC, (1969) On the response of beams to an arbitrary number of concentrated moving masses. J Franklin Inst 287(2):115–123
Thai H-T, Vo TP (2012) Bending and free vibration of functionally graded beams using various higher-order shear deformation beam theories. Int J Mech Sci 62(1):57–66
Tian Y, Li Q, Feng Y, Yu Y, Wu D, Chen X, Gao W (2023) Nonlinear dynamic analysis of the functionally graded graphene platelets

reinforced porous plate under moving mass. Thin-Walled Struct 183:110363

Tran M-T, Nguyen V-L, Trinh A-T (2017) Static and vibration analysis of cross-ply laminated composite doubly curved shallow shell panels with stiffeners resting on Winkler-Pasternak elastic foundations. Int J Adv Struct Eng 9(2):153–164

Tung PT, Long NV, Tu TM, Phuong NTB, Hai LT, Long TN (2021) Nonlinear bending analysis of fgp plates under various boundary conditions using an analytical approach. Structures 34:4803–4813

Van Vinh P, Duoc NQ, Phuong ND (2022) A new enhanced first-order beam element based on neutral surface position for bending analysis of functionally graded porous beams. Iran J Sci Technol, Trans Mech Eng 46(4):1141–1156

Vu ANT, Le NAT, Nguyen DK (2021) Dynamic behaviour of bidirectional functionally graded sandwich beams under a moving mass with partial foundation supporting effect. Acta Mech 232(7):2853–2875

Wang C, Reddy JN, Lee K (2000) Shear deformable beams and plates: Relationships with classical solutions. Elsevier, UK

Wang Y, Xie K, Fu T, Shi C (2019) Vibration response of a functionally graded graphene nanoplatelet reinforced composite beam under two successive moving masses. Compos Struct 209:928–939

Wang Y, Zhou A, Fu T, Zhang W (2020) Transient response of a sandwich beam with functionally graded porous core traversed by a non-uniformly distributed moving mass. Int J Mech Mater Des 16(3):519–540

Xie K, Wang Y, Fan X, Fu T (2020) Nonlinear free vibration analysis of functionally graded beams by using different shear deformation theories. Appl Math Model 77:1860–1880